Line-profile approach to the description of the electron-recombination process for the highly charged ions

O. Yu. Andreev,[1] L. N. Labzowsky,[1,2] and A. V. Prigorovsky[1]
[1]*Faculty of Physics, St. Petersburg State University, Ulyanovskaya 1, Petrodvorets, St. Petersburg 198504, Russia*
[2]*Petersburg Nuclear Physics Institute, Gatchina, St. Petersburg 188300, Russia*
(Received 17 August 2009; published 22 October 2009)

The line-profile approach is applied to the evaluation of the electron recombination on the highly charged ions within the framework of QED. Both dielectronic recombination and radiative recombination processes are considered. The interelectron interaction is taken into account partly to all orders of the QED perturbation theory. The radiative corrections to the lowest order (the electron self-energy and the vacuum polarization) are also included. With this approach the most accurate contemporary results for the electron-recombination cross section on the one-electron uranium ion are obtained; these results are compared with the earlier calculations and with existing experimental data.

DOI: 10.1103/PhysRevA.80.042514 PACS number(s): 31.10.+z, 31.15.ac, 31.30.J−

I. INTRODUCTION

Dielectronic recombination (DR) or inverse autoionization process is known since the work of Massey and Bates [1], where the recombination of an electron with O^+ ion was investigated. DR plays a fundamental role in the determination of the level populations and ionization balance of high-temperature laboratory and astrophysical plasma. The development of ion accelerators, electron beam ion traps (EBITs), and storage rings has made possible the observation of increasingly more detailed and complex DR spectra [2–5]. From DR experiments one can obtain precise knowledge of the resonance energies of doubly excited states and collision dynamics. The branching ratios in the capture and deexcitation processes become experimentally accessible as well. The measurement of resonance line shapes in the highly charged ions (HCIs) provides the information on the velocity distribution of the cooler electron beam and the natural linewidths.

There are also rather numerous theoretical calculations of the DR effect in HCI [6–15] (see also [16,17]). For numerical calculations the different theoretical methods were applied: the versions of the multiconfigurational Dirac-Fock approach [6–8,14,15,18] and quantum electrodynamical perturbation theory (QED PT) approach [9–13]. In this work we apply more accurate QED approach, namely, line-profile approach (LPA) [16,19–21] to the calculation of the DR process in HCI. Within this approach the interelectron interaction is partly included to all orders in QED PT. Also partly we include radiative corrections to the DR process. As an example a DR process on the H-like uranium ion will be evaluated. This gives a possibility to compare the results with the earlier calculations in [9,15].

The process of recombination of an electron with one-electron uranium ion looks like

$$e(\epsilon_e) + \mathrm{U}^{91+}(1s) \to \mathrm{U}^{90+}(1s1s) + \gamma(\omega). \tag{1}$$

In this process the initial state of the system is presented by a one-electron ion of uranium $[\mathrm{U}^{91+}(1s)]$ in the ground state and an incident electron $[e(\epsilon_e)]$ with energy ϵ_e. The final state is a two-electron ion of uranium $[\mathrm{U}^{90+}(1s1s)]$ in the ground state and emitted photon or a set of emitted photons with total energy defined by the energy conservation law.

If the process of electron recombination is registered by detection of a photon with frequency $\omega \approx \epsilon_e + \epsilon_{1s} - E_r$, where E_r is the energy of a two-electron single excited configuration (r), then the electron recombination is determined by two particular processes,

$$e(\epsilon_e) + \mathrm{U}^{91+}(1s) \to \mathrm{U}^{90+}(r) + \gamma(\omega) \to \cdots \tag{2}$$

and

$$e(\epsilon_e) + \mathrm{U}^{91+}(1s) \to \mathrm{U}^{90+}(d) \to \mathrm{U}^{90+}(r) + \gamma(\omega) \to \cdots, \tag{3}$$

where d designates a double excited configuration. Contribution of the neglected (multiphoton) processes to the electron-recombination cross section is a small correction [15]. The process [Eq. (2)] is called radiative recombination (RR). Below the threshold of the two-electron excitation RR process fully defines the recombination cross section. Above the threshold of the two-electron excitation the RR process is always seen together with the process of DR given by Eq. (3).

The cross section of electron recombination considered as a function of the incident electron energy (ϵ_e) reveals resonances in the area where sum of the incident electron and $1s$-electron energies $(\epsilon_e + \epsilon_{1s})$ is close to the energies of double excited two-electron configurations. The DR process is the dominant process contributing to the cross section in the resonance areas. The RR process is nonresonant. In this work we will consider double excited configurations with $2s$ and $2p$ electrons only. Accordingly, the double excited two-electron configuration (d) is one of the $(2s2s)$, $(2s2p)$, and $(2p2p)$ configurations. The single excited two-electron configuration (r) is one of the $(1s2s)$ and $(1s2p)$ configurations. The frequency ω of emitted photon $\gamma(\omega)$ is defined by the energy conservation law. If the energy of the initial state is equal to the energy of an excited two-electron configuration (only the double excited configurations can fit this condition) the cross section shows a resonance.

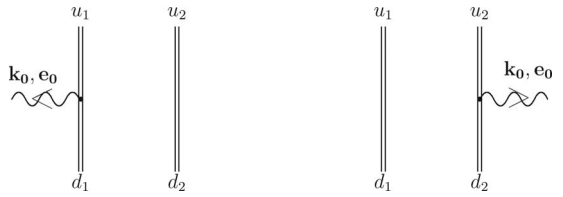

FIG. 1. The Feynman graphs representing the process of electron recombination in the zero order of perturbation theory. The double solid line corresponds to the bound electrons; the wavy lines with the arrows describe the emission of the photons. The indices d_1, d_2 correspond to the initial one-electron states of a system; u_1, u_2 correspond to the final states.

In the resonance area both processes [Eqs. (2) and (3)] constitute a single process of the electron capture by the ion, being the nonresonant and resonant parts of this process, respectively (though DR is dominating). If the standard QED perturbation theory is employed, then the lowest order of the QED PT (see Fig. 1) corresponds to the pure RR process. The next order of the QED PT (see Fig. 2) presents already both RR and DR processes. Accordingly, the contribution of the RR process to the cross section in the resonance area can be separated only in the lowest order of the standard QED PT. Beyond the standard QED PT, as in the present work, the contributions of the RR and DR processes to the total cross section become inseparable.

II. APPLICATION OF THE LINE-PROFILE APPROACH

The process of electron recombination to the single excited configuration (r) can be considered as a transition

$$I \to F, \tag{4}$$

where the initial state (I) corresponds to two electrons: a bound $1s$ electron and an incident electron, i.e., continuum electron. The final state (F) corresponds to the two bound electrons ($1s$ electron and either $2s$ or $2p$ electron) composing a two-electron configuration.

To the lowest orders of QED PT this process is described by the Feynman graphs depicted in Figs. 1 and 2. The corresponding calculation was performed in [9,12]. The aim of the present work is to develop *ab initio* QED method which allows for improvement of the accuracy of the calculations

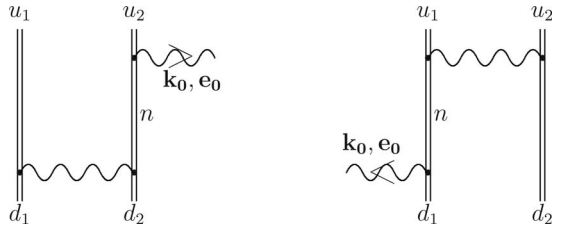

FIG. 2. The Feynman graphs representing the first-order interelectron interaction corrections to the process of electron recombination. The internal wavy line denotes the exchange by the photon between two electrons. The meaning of the indices u_1, u_2, d_1, and d_2 is the same as in Fig. 1; the index n corresponds to the intermediate one-electron states.

by taking into account the interelectron interaction more precisely. For calculation of the higher order interelectron interaction corrections we employ the LPA [16,21].

The application of the LPA to the calculation of transition probabilities is presented in detail in [21]. The technique developed in [21] can be utilized only for the bound electrons. Since in our case the initial state contains a continuum electron, we will introduce an auxiliary bound electron system which properties are explicitly related to the properties of original system.

We will designate the wave function of the continuum electron as $\psi_e(\boldsymbol{r})$. First we introduce a function

$$\psi_{e_R}^{(\mathrm{aux})}(\boldsymbol{r}) = \psi_e(\boldsymbol{r})\,\theta(R - |\boldsymbol{r}|), \tag{5}$$

where $\theta(R-|\boldsymbol{r}|)$ is the Heaviside step function. The function $\psi_{e_R}^{(\mathrm{aux})}(\boldsymbol{r})$ coincides with the function $\psi_e(\boldsymbol{r})$ for $|\boldsymbol{r}|<R$ and is set to zero for $|\boldsymbol{r}|>R$. The function $\psi_{e_R}^{(\mathrm{aux})}(\boldsymbol{r})$ can be normalized to unity. The corresponding normalization factor N_R and the normalized function $\psi_{e_R}(\boldsymbol{r})$ read

$$N_R = \left[\int d^3\boldsymbol{r} |\psi_{e_R}^{(\mathrm{aux})}(\boldsymbol{r})|^2\right]^{1/2}, \tag{6}$$

$$\psi_{e_R}(\boldsymbol{r}) = \frac{\psi_{e_R}^{(\mathrm{aux})}(\boldsymbol{r})}{N_R}. \tag{7}$$

Note that for the large R values the normalization factor N_R is proportional to $\sqrt{R}$ and, accordingly,

$$\psi_{e_R}(\boldsymbol{r}) \sim \frac{1}{\sqrt{R}}. \tag{8}$$

We can introduce an artificial bound electron state e_R described by the wave function ψ_{e_R}. The energies and the angular quantum numbers of the continuum electron state ψ_e and the bound electron state ψ_{e_R} are equal. Consider now two processes described by Eq. (4) which differ by the initial states. The first initial state is $1s$ electron and the continuum electron e. The second initial state is $1s$ electron and the artificial bound electron e_R. The amplitude of the first process (U) and the amplitude of the second process (U_R) are related like

$$U = \lim_{R\to\infty} N_R U_R. \tag{9}$$

Accordingly, we can generalize the LPA for calculation of the amplitude of the process of electron recombination. We employ the artificial bound electron state e_R defined by Eq. (7) and apply the LPA for calculation of the transition amplitude (U_R), i.e., for the system where the continuum electron is substituted by the bound electron e_R. The amplitude of the process of electron recombination is given by Eq. (9). The limit $R\to\infty$ can be evaluated numerically. This procedure has an explicit physical meaning which is explained in Appendix A.

III. CROSS SECTION

We consider process of electronic recombination with one-electron ion. Initial state is presented by two electrons:

bound electron and incident electron (electron in the continuous Dirac spectrum). The final state is a single excited two-electron configuration [for example, $(1s2s)$ or $(1s2p)$] and emitted photon.

The photon is described by momentum $(\boldsymbol{k})$, frequency $(\omega=|\boldsymbol{k}|)$, and polarization (λ). It is also convenient to introduce photon wave vector $\boldsymbol{\nu}_k=\boldsymbol{k}/|\boldsymbol{k}|$. Normalization of the photon wave function $[A=(A^0,\boldsymbol{A})]$, corresponding to one particle per unit volume, is

$$\int d^3\boldsymbol{r}A^{(\boldsymbol{k},\lambda)+}(\boldsymbol{r})A^{(\boldsymbol{k}',\lambda')}(\boldsymbol{r})=(2\pi)^3\frac{4\pi}{2\omega}\delta(\boldsymbol{k}-\boldsymbol{k}')\delta_{\lambda,\lambda'}. \tag{10}$$

We employ relativistic unit system, where the fine-structure constant is $\alpha=e^2$, e is the electron charge.

The bound electron is described by the principal quantum number n_b, the total angular momentum (j_b), its projection (m_b), and parity (l_b). The wave function of the bound electron is designated as $\psi_{n_bj_bl_bm_b}(\boldsymbol{r})$.

The incident electron is characterized by momentum $(\boldsymbol{p})$, energy (ϵ), and polarization or spin projection (μ) and is described by wave function $\psi_{\boldsymbol{p}\mu}(\boldsymbol{r})$. The energy, the momentum, and the electron mass (m_e) are connected as $\epsilon=\sqrt{p^2+m_e^2}$, where $p=|\boldsymbol{p}|$. It is also convenient to introduce the electron wave vector $\boldsymbol{\nu}_p=\boldsymbol{p}/|\boldsymbol{p}|$. The wave function of incident electron is normalized like

$$\int d^3\boldsymbol{r}\psi^+_{\boldsymbol{p}'\mu'}(\boldsymbol{r})\psi_{\boldsymbol{p}\mu}(\boldsymbol{r})=(2\pi)^3\delta^3(\boldsymbol{p}'-\boldsymbol{p})\delta_{\mu'\mu} \tag{11}$$

$$=\frac{(2\pi)^3}{p\epsilon}\delta(\epsilon'-\epsilon)\delta(\cos\theta'-\cos\theta)\delta(\phi'-\phi)\delta_{\mu'\mu}, \tag{12}$$

where the set (p,θ,ϕ) represents the vector $\boldsymbol{p}$ in spherical coordinates. This normalization corresponds to one particle per unit volume.

The electron wave function with certain momentum and polarization can be expanded in the wave functions with certain energy (ε, which runs over the Dirac spectrum), total angular momentum (j), parity (l), and projection of the total angular momentum (m). These functions are designated as $\psi_{\varepsilon jlm}(\boldsymbol{r})$ and are normalized like

$$\int d^3\boldsymbol{r}\psi^+_{\varepsilon'j'l'm'}(\boldsymbol{r})\psi_{\varepsilon jlm}(\boldsymbol{r})=\delta(\varepsilon'-\varepsilon)\delta_{j'j}\delta_{l'l}\delta_{m'm}. \tag{13}$$

Accordingly, we can write

$$\psi_{\boldsymbol{p}\mu}(\boldsymbol{r})=\int d\varepsilon\sum_{jlm}a_{\boldsymbol{p}\mu,\varepsilon jlm}\psi_{\varepsilon jlm}(\boldsymbol{r}), \tag{14}$$

where the matrix element $a_{\boldsymbol{p}\mu,\varepsilon jlm}$ is given by

$$a_{\boldsymbol{p}\mu,\varepsilon jlm}=\int d^3\boldsymbol{r}\psi^+_{\varepsilon jlm}(\boldsymbol{r})\psi_{\boldsymbol{p}\mu}(\boldsymbol{r}). \tag{15}$$

Introducing coefficients

$$\alpha_{\boldsymbol{\nu}_p\mu,jlm}=[\Omega^+_{jlm}(\boldsymbol{\nu}_p)v^\mu(\boldsymbol{\nu}_p)], \tag{16}$$

where $\Omega_{jlm}(\boldsymbol{\nu}_p)$ is the spherical spinor and $v^\mu(\boldsymbol{\nu}_p)$ is the unit spinor function, the matrix elements $a_{\boldsymbol{p}\mu,\epsilon'jlm}$ can be written in the form

$$a_{\boldsymbol{p}\mu,\varepsilon jlm}=\frac{(2\pi)^{3/2}}{\sqrt{p\epsilon}}\delta(\varepsilon-\epsilon)e^{i\varphi_{jl}}\alpha_{\boldsymbol{\nu}_p\mu,jlm}, \tag{17}$$

where the phase φ_{jl} is determined by the field of the nucleus [22]. The orthonormality conditions for coefficients $\alpha_{\boldsymbol{\nu}_p\mu,jlm}$ read [23]

$$\sum_{jlm}\alpha^*_{\boldsymbol{\nu}'_p\mu',jlm}\alpha_{jlm,\boldsymbol{\nu}_p\mu}=\delta(\cos\theta'-\cos\theta)\delta(\phi'-\phi)\delta_{\mu'\mu} \tag{18}$$

and

$$\int d^2\boldsymbol{\nu}_p\sum_\mu\alpha^*_{j'l'm',\boldsymbol{\nu}_p\mu}\alpha_{\boldsymbol{\nu}_p\mu,jlm}=\delta_{j'j}\delta_{l'l}\delta_{m'm}. \tag{19}$$

Then, the matrix elements $a_{\varepsilon jlm,\boldsymbol{p}\mu}$ satisfy the following normalization conditions:

$$\int d\varepsilon\sum_{jlm}a^*_{\boldsymbol{p}'\mu',\varepsilon jlm}a_{\varepsilon jlm,\boldsymbol{p}\mu}=(2\pi)^3\delta^3(\boldsymbol{p}-\boldsymbol{p}') \tag{20}$$

and

$$\int d^3\boldsymbol{p}\sum_\mu a^*_{\varepsilon'j'l'm',\boldsymbol{p}\mu}a_{\boldsymbol{p}\mu,\varepsilon jlm}=(2\pi)^3\delta(\varepsilon-\varepsilon')\delta_{j'j}\delta_{l'l}\delta_{m'm}. \tag{21}$$

Accordingly, we get

$$\int d\varepsilon d\varepsilon'\int d^2\boldsymbol{\nu}_p\sum_\mu a^*_{\varepsilon'j'l'm',\boldsymbol{p}\mu}a_{\boldsymbol{p}\mu,\varepsilon jlm}U^*_{\varepsilon'j'l'm'}U_{\varepsilon jlm}$$
$$=\frac{(2\pi)^3}{p\epsilon}\delta_{j'j}\delta_{l'l}\delta_{m'm}|U_{\epsilon jlm}|^2. \tag{22}$$

Here, $U_{\varepsilon jlm}$ is an arbitrary function of ε, j, l and m.

The two-electron wave function for the initial sate of the system can be composed as

$$\Psi_{\boldsymbol{p}\mu n_bj_bl_bm_b}(\boldsymbol{r}_1,\boldsymbol{r}_2)$$
$$=\frac{1}{\sqrt{2}}[\psi_{\boldsymbol{p}\mu}(\boldsymbol{r}_1)\psi_{n_bj_bl_bm_b}(\boldsymbol{r}_2)-\psi_{n_bj_bl_bm_b}(\boldsymbol{r}_1)\psi_{\boldsymbol{p}\mu}(\boldsymbol{r}_2)], \tag{23}$$

where functions $\psi_{n_bj_bl_bm_b}$ and $\psi_{\boldsymbol{p}\mu}$ are eigenvectors of the Dirac equation: bound electron with the principal quantum number (n_b), total angular momentum j_b, its projection m_b, parity l_b, and an electron with momentum and polarization $(\boldsymbol{p},\mu)$, respectively.

The final state is presented by photon $(\boldsymbol{k},\lambda)$ and a single excited configuration (r) written in the j-j coupling scheme,

$$\Psi_r(\boldsymbol{r}_1,\boldsymbol{r}_2)=\Psi_{J_rM_rn_{r1}j_{r1}l_{r1}n_{r2}j_{r2}l_{r2}}(\boldsymbol{r}_1,\boldsymbol{r}_2), \tag{24}$$

where

$$\Psi_{JMn_1j_1l_1n_2j_2l_2}(\boldsymbol{r}_1,\boldsymbol{r}_2) = N\sum_{m_1m_2} C^{j_1j_2}_{JM}(m_1,m_2) \times[\psi_{n_1j_1l_1m_1}(\boldsymbol{r}_1)\psi_{n_2j_2l_2m_2}(\boldsymbol{r}_2) - \psi_{n_2j_2l_2m_2}(\boldsymbol{r}_1)\psi_{n_1j_1l_1m_1}(\boldsymbol{r}_2)]. \quad (25)$$

Here, J, M are the total angular momentum of a two-electron system and its projection, normalization constant N is equal to $1/\sqrt{2}$ for nonidentical electrons and to 1/2 for identical electrons, and $C^{j_1j_2}_{JM}(m_1,m_2)$ are the Clebsch-Gordan coefficients. In the single excited configurations one of the electrons is $1s$ electron, another is $2s$ or $2p$ electron (we do not consider higher excitations).

The amplitude of the process (U_{if}) is defined via S matrix,

$$S_{if} = (-2\pi i)\delta(E_f - E_i)U_{if}. \quad (26)$$

Then, the transition probability is given by [22]

$$dw_{if} = 2\pi|U_{if}|^2\delta(E_f - E_i)\frac{d^3\boldsymbol{k}}{(2\pi)^3}, \quad (27)$$

where E_i, E_f are the initial and final energies of the whole system. Factor $d^3\boldsymbol{k}/(2\pi)^3$ gives the number of photon states with certain polarization and momentum within interval $d^3\boldsymbol{k}$ per unit volume: $d^3\boldsymbol{k}/[n^{\mathrm{ph}}(2\pi)^3]$, where the photon density (n^{ph}) is set equal to unity [see Eq. (10)].

Cross section is connected with the transition probability [Eq. (27)] as [22]

$$d\sigma_{if} = \frac{dw_{if}}{j}, \quad (28)$$

where j is the current of the incident electron. This current is defined as $j = n^{\mathrm{el}}v$, where n^{el} and $v = p/\epsilon$ are the density and velocity of the incident electron, respectively, in the rest system of the nucleus. With the normalization equation [Eq. (11)] the electron density is equal to unity. Accordingly, the cross section reads

$$d\sigma_{if} = 2\pi\frac{\epsilon}{p}|U_{\boldsymbol{p}\mu n_bj_bl_bm_b,\boldsymbol{k}\lambda r}|^2\delta(E_f - E_i)\frac{d^3\boldsymbol{k}}{(2\pi)^3}. \quad (29)$$

The initial ($\boldsymbol{p}\mu n_bj_bl_bm_b$) and final ($r$) state configurations are defined by Eqs. (23) and (24), respectively, $\boldsymbol{k}$ and λ represent the photon quantum numbers.

Employing Eq. (14) we get

$$d\sigma_{if} = 2\pi\frac{\epsilon}{p}\left|\int d\varepsilon\sum_{jlm} a_{\boldsymbol{p}\mu,\varepsilon jlm}U_{\varepsilon jlmn_bj_bl_bm_b,\boldsymbol{k}\lambda r}\right|^2 \times\delta(E_f - E_i)\frac{d^3\boldsymbol{k}}{(2\pi)^3}, \quad (30)$$

where the wave function for configuration ($\varepsilon jlmn_bj_bl_bm_b$) is defined as

$$\Psi_{\varepsilon jlmn_bj_bl_bm_b}(\boldsymbol{r}_1,\boldsymbol{r}_2) = \frac{1}{\sqrt{2}}[\psi_{\varepsilon jlm}(\boldsymbol{r}_1)\psi_{n_bj_bl_bm_b}(\boldsymbol{r}_2) - \psi_{n_bj_bl_bm_b}(\boldsymbol{r}_1)\psi_{\varepsilon jlm}(\boldsymbol{r}_2)]. \quad (31)$$

In this work we calculate the full cross section of the electronic recombination, which means the integration over the directions of the emitted photon ($\boldsymbol{\nu}_k$) and summation over the photon polarization (λ). Then, we suppose that the incident electron is not polarized, hence, we average over the electron polarization (μ). Accordingly, we can also average over the electron momentum direction ($\boldsymbol{\nu}_p$) and over the total angular momentum projection of the bound electron in the initial state (m_b). The average over $\boldsymbol{\nu}_p$, μ, and m_b means

$$\frac{1}{8\pi(2j_b+1)}\int d^2\boldsymbol{\nu}_p\sum_{\mu m_b}. \quad (32)$$

The summation over electron polarization and the integration over electron momentum direction are performed with employment of Eq. (22). Accordingly, we get

$$d\sigma_{if} = 2\pi\frac{\epsilon}{p}\frac{1}{8\pi(2j_b+1)}\frac{(2\pi)^3}{p\epsilon}\sum_{jlmm_b}|U_{\epsilon jlmn_bj_bl_bm_b,\boldsymbol{k}\lambda r}|^2 \times\delta(E_f - E_i)\frac{d^3\boldsymbol{k}}{(2\pi)^3}. \quad (33)$$

It is convenient to substitute summation over configurations in j-j coupling scheme [Eq. (25)] for the summation over configurations [Eq. (31)]. Then, using the Clebsch-Gordan transformation (which is a unitary transformation) we yield

$$d\sigma_{if} = 2\pi\frac{\epsilon}{p}\frac{1}{8\pi(2j_b+1)}\frac{(2\pi)^3}{p\epsilon}\sum_{JMjl}|U_{JM\epsilon jln_bj_bl_b,\boldsymbol{k}\lambda r}|^2 \times\delta(E_f - E_i)\frac{d^3\boldsymbol{k}}{(2\pi)^3}, \quad (34)$$

where configuration ($JM\epsilon jln_bj_bl_b$) is defined as

$$\Psi_{JM\epsilon jln_bj_bl_b}(\boldsymbol{r}_1,\boldsymbol{r}_2) = \frac{1}{\sqrt{2}}\sum_{mm_b} C^{jj_b}_{JM}(m,m_b) \times[\psi_{\epsilon jlm}(\boldsymbol{r}_1)\psi_{n_bj_bl_bm_b}(\boldsymbol{r}_2) - \psi_{n_bj_bl_bm_b}(\boldsymbol{r}_1)\psi_{\epsilon jlm}(\boldsymbol{r}_2)]. \quad (35)$$

We calculate cross section for the electron recombination to any single excited two-electron configuration; accordingly, we have to sum over all the single excited configurations (r) in the final state [see Eq. (24)]. In Table I we list the transitions between $(n_bl_{bj_b},\epsilon l_j)_{JM}$ and $r=(n_{r1}l_{r1j_{r1}},n_{r2}l_{r2j_{r2}})_{J_rM_r}$ two-electron configurations, written in the j-j coupling scheme, taken into account. In principle, we have to sum over the total angular momentum projections (M,M_r). Actually, we calculate the transitions with certain projections M, M_r (given in the second column of Table I) and, then,

TABLE I. Transitions between $(n_b l_{b j_b}, \epsilon l_j)_{JM}$ and $r=(n_{r1} l_{r1 j_{r1}}, n_{r2} l_{r2 j_{r2}})_{J_r M_r}$, two-electron configurations in j-j coupling scheme considered in this work. Contribution of the listed transitions to the total cross section is calculated as contribution of the transitions with certain total angular momentum projections (M, M_r) multiplied by the factor f, respectively.

Transition	$M \to M_r$	f
$(1s, \epsilon s_{1/2})_0 \to (1s2p_{1/2})_1$	$0 \to 0$	3
$(1s, \epsilon s_{1/2})_0 \to (1s2p_{3/2})_1$	$0 \to 0$	3
$(1s, \epsilon s_{1/2})_1 \to (1s2p_{1/2})_0$	$0 \to 0$	3
$(1s, \epsilon s_{1/2})_1 \to (1s2p_{1/2})_1$	$1 \to 1$	6
$(1s, \epsilon s_{1/2})_1 \to (1s2p_{3/2})_1$	$1 \to 1$	6
$(1s, \epsilon s_{1/2})_1 \to (1s2p_{3/2})_2$	$0 \to 0$	15/2
$(1s, \epsilon p_{1/2})_0 \to (1s2s_{1/2})_1$	$0 \to 0$	3
$(1s, \epsilon p_{1/2})_1 \to (1s2s_{1/2})_0$	$0 \to 0$	3
$(1s, \epsilon p_{1/2})_1 \to (1s2s_{1/2})_1$	$1 \to 1$	6
$(1s, \epsilon p_{3/2})_1 \to (1s2s_{1/2})_0$	$0 \to 0$	3
$(1s, \epsilon p_{3/2})_1 \to (1s2s_{1/2})_1$	$1 \to 1$	6
$(1s, \epsilon p_{3/2})_2 \to (1s2s_{1/2})_1$	$0 \to 0$	15/2
$(1s, \epsilon d_{3/2})_1 \to (1s2p_{1/2})_0$	$0 \to 0$	3
$(1s, \epsilon d_{3/2})_1 \to (1s2p_{1/2})_1$	$1 \to 1$	6
$(1s, \epsilon d_{3/2})_1 \to (1s2p_{3/2})_1$	$1 \to 1$	6
$(1s, \epsilon d_{3/2})_1 \to (1s2p_{3/2})_2$	$0 \to 0$	15/2
$(1s, \epsilon d_{3/2})_2 \to (1s2p_{1/2})_1$	$0 \to 0$	15/2
$(1s, \epsilon d_{3/2})_2 \to (1s2p_{3/2})_1$	$0 \to 0$	15/2
$(1s, \epsilon d_{3/2})_2 \to (1s2p_{3/2})_2$	$2 \to 2$	15/2
$(1s, \epsilon d_{5/2})_2 \to (1s2p_{1/2})_1$	$0 \to 0$	15/2
$(1s, \epsilon d_{5/2})_2 \to (1s2p_{3/2})_1$	$0 \to 0$	15/2
$(1s, \epsilon d_{5/2})_2 \to (1s2p_{3/2})_2$	$2 \to 2$	15/2
$(1s, \epsilon d_{5/2})_3 \to (1s2p_{3/2})_2$	$0 \to 0$	35/3

multiply them by a factor f (the third column of Table I), which accounts for contribution of all the other projections for the same transitions.

Finally, after integration over the photon frequency we get

$$d\sigma_{if} = \frac{\omega^2}{(2\pi)^2}\left[\frac{\pi^2}{(2j_b+1)p^2}\right]\int d^2\boldsymbol{\nu}_k \sum_{JMjlr} |U_{JM\epsilon jln_b j_b l_b, \boldsymbol{k}\lambda r}|^2, \tag{36}$$

where the photon frequency (ω) is defined now by the energy conservation law. Integration over directions of the emitted photon and summation over the polarization are performed in the standard way. Expression (36) differs from expression for the transition probabilities employed in [21] by the factor in the square brackets.

IV. NUMERICAL METHODS

In the numerical calculations an ion is considered to be enclosed into a spherical box with the radius $R^{\mathrm{box}}=70/(\alpha Z)$ (in the relativistic units), where α is the fine-structure constant and Z is the nuclear charge. The Dirac spectrum in the external field of the nucleus is constructed in terms of B splines [24,25]. We used B splines of order 8 and a grid with 60 nonzero knots. Hence, the generated electron spectrum is discrete and finite. The eigenvector and the corresponding eigenvalue (i.e., energy), which is the most close to the energy of the incident electron (ϵ_e), are substituted by the function ψ_{e_R} [see Eq. (7)] and by the energy ϵ_e, respectively. The electron states of the generated spectrum, which are the next to the substituted electron state (e_n), are designated as e_{n-1} and e_{n+1}. Enlargement of the box and the number of the knots reduce the effect of the substitution of the incident electron state (ϵ_e) for the e_n state. The size of the box and the number of the knots are chosen to be large enough not to influence the accuracy of the calculation.

Within the framework of the LPA the properties of an ion are derived from the line profile associated with the process of elastic photon scattering on an ion, where an ion in the ground state absorbs and emits a photon. The resonances of this scattering process correspond to the energy levels. In order to describe an energy level by two parameters (energy and width) we parametrize the line profile by a Lorentz contour, which is determined by the position of the resonance (i.e., energy) and its width. For details concerning the LPA and its application to the evaluation of energies we refer to [19,20]. The application of the LPA to the evaluation of transition probabilities is presented in [16,21].

Within the framework of the LPA the energy levels are derived from the matrix V, which is evaluated with employment of the QED perturbation theory order by order,

$$V(\omega) = V^{(0)} + \Delta V^{(1)}(\omega) + \Delta V^{(2)}(\omega) + \cdots. \tag{37}$$

The matrix $V(\omega)$ depends on ω, which has a physical meaning of the scattered photon frequency. The matrix $V^{(0)}$ contains the corresponding one-electron Dirac energies. The matrix $V^{(1)}(\omega)$ includes the first-order corrections, such as self-energy (SE) and vacuum polarization (VP) corrections, and one-photon exchange corrections. The matrix $V^{(2)}(\omega)$ includes the second-order corrections such as two-photon exchange corrections ("box" and "cross" graphs), SE and VP screening corrections, two-loop SE, VP corrections, etc. In this work the matrix V includes only the first-order corrections: one-photon exchange corrections, SE and VP corrections. However, the irreducible parts of the higher order corrections will be partly taken into account in our approach (see below). The inclusion of the SE corrections provides the width of the levels determined by these corrections. The photon exchange graphs via their imaginary parts provide also the Auger width.

The one-photon exchange operator (acting on two-electron functions represented by antisymmetric combination of one-electron functions) can be written as

$$\Delta V^{1\mathrm{ph}}_{u_1 u_2 d_1 d_2} = I(|\varepsilon_{u_2} - \varepsilon_{d_2}|)_{u_1 u_2 d_1 d_2}, \tag{38}$$

where

TABLE II. The complex matrix elements of the SE and VP operators in eV employed in this work. The matrix elements for s electrons are calculated in this work; the accuracy is given in round brackets. The other diagonal matrix elements are taken from [29,30,32].

$\langle 1s_{1/2}\|\hat{\Sigma}(1s_{1/2})\|1s_{1/2}\rangle$	(354.99(5),0)	$\langle 1s_{1/2}\|\hat{V}^{\rm VP}\|1s_{1/2}\rangle$	−88.63
$\langle 2s_{1/2}\|\hat{\Sigma}(2s_{1/2})\|2s_{1/2}\rangle$	(65.40(2),−0.06(1))	$\langle 2s_{1/2}\|\hat{V}^{\rm VP}\|2s_{1/2}\rangle$	−15.65
$\langle 2p_{1/2}\|\hat{\Sigma}(2p_{1/2})\|2p_{1/2}\rangle$	(9.55,−15.54(1))	$\langle 2p_{1/2}\|\hat{V}^{\rm VP}\|2p_{1/2}\rangle$	−2.70
$\langle 2p_{3/2}\|\hat{\Sigma}(2p_{3/2})\|2p_{3/2}\rangle$	(8.90,−13.03(1))	$\langle 2p_{3/2}\|\hat{V}^{\rm VP}\|2p_{3/2}\rangle$	−0.10
$\langle 1s_{1/2}\|\hat{\Sigma}(1s_{1/2})\|2s_{1/2}\rangle$	(136.41(3),0)	$\langle 1s_{1/2}\|\hat{V}^{\rm VP,Uehl}\|2s_{1/2}\rangle$	−39.16(1)
$\langle 1s_{1/2}\|\hat{\Sigma}(2s_{1/2})\|2s_{1/2}\rangle$	(165.60(3),22.30(1))	$\langle 1s_{1/2}\|\hat{V}^{\rm VP,Uehl}\|2s_{1/2}\rangle$	−39.16(1)

$$I_{u_1u_2d_1d_2}(\Omega)=\sum_{\mu_1\mu_2=0}^{3}\int d^3\boldsymbol{r}_1 d^3\boldsymbol{r}_2\bar{\psi}_{u_1}(\boldsymbol{r}_1)\bar{\psi}_{u_2}(\boldsymbol{r}_2)\times\gamma_1^{\mu_1}\gamma_2^{\mu_2}I_{\mu_1\mu_2}(\Omega,r_{12})\psi_{d_1}(\boldsymbol{r}_1)\psi_{d_2}(\boldsymbol{r}_2),\quad(39)$$

u_1, u_2, d_1, d_2 designate one-electron Dirac states, and ε_{u_2}, ε_{d_2} are the one-electron Dirac energies. Dirac matrices $\gamma_i^{\mu_i}$ act on the one-electron functions $\psi_{d_i}(\boldsymbol{r}_i)$. Function $I_{\mu_1\mu_2}(\Omega,r_{12})$ looks like

$$I_{\mu_1\mu_2}(\Omega,r_{12})=\frac{\delta_{\mu_1 0}\delta_{\mu_2 0}}{r_{12}}\quad(40)$$

$$-\left(\frac{\delta_{\mu_1\mu_2}}{r_{12}}e^{i\Omega r_{12}}+\frac{\partial}{\partial x_1^{\mu_1}}\frac{\partial}{\partial x_2^{\mu_2}}\frac{1}{r_{12}}\frac{1-e^{i\Omega r_{12}}}{\Omega^2}\right)\times(1-\delta_{\mu_1 0})(1-\delta_{\mu_2 0})\quad(41)$$

if Coulomb gauge is employed or

$$I_{\mu_1\mu_2}(\Omega,r_{12})=\frac{g_{\mu_1\mu_2}}{r_{12}}e^{i\Omega r_{12}}\quad(42)$$

if Feynman gauge is employed. Tensor $g_{\mu_1\mu_2}$ is the metric tensor, $\delta_{\mu_1\mu_2}$ is the Kronecker delta, and $r_{12}=|\boldsymbol{r}_1-\boldsymbol{r}_2|$.

The matrix elements of the SE and VP operators are given in Table II. The SE matrix elements were evaluated within the Snyderman version of the standard QED PT approach [26–28] for the tightly bound electrons. For details see Appendix A. We calculated the nondiagonal SE matrix elements and the imaginary part of the matrix elements. The real part of the diagonal SE matrix elements is taken from [29,30]. The VP matrix elements are divided into the Uehling part and the Wichmann-Kroll part [31]. The Uehling part, i.e., the matrix elements of the Uehling potential (see, for example, [22]), is calculated in this work; the Wichmann-Kroll part is borrowed from [32]. The Coulomb-Dirac wave functions for extended nucleus with Fermi distribution are employed. The root mean square radius is $r_{\rm rms}=5.860$ fm.

The amplitude of the transition process from the initial state I to the final state F with emission of a photon with the frequency ω_0 can be written as

$$U_{I\to F}=[\Xi(\omega_0)]_{\Phi_F\Phi_I},\quad(43)$$

where Φ_I and Φ_F are the eigenvectors of the matrix $V(\omega)$ corresponding to the I and F states, respectively. The operator $\Xi(\omega_0)$ is evaluated with employment of the QED PT (see [16,21]). In zero order approximation this operator coincides with the photon emission operator ($A^{(k_0,\lambda_0)*}$). In this work we consider only the one-photon exchange corrections to the operator Ξ. According to [21], it reads

$$\Xi=\Xi^{(0)}+\Xi^{(1)}+eO(\alpha^2),\quad(44)$$

where

$$\Xi^{(0)}_{u_1u_2d_1d_2}=2eA^{(k_0,\lambda_0)*}_{u_1d_1}\delta_{u_2d_2},\quad(45)$$

$$\Xi^{(1)}_{u_1u_2d_1d_2}=\sum_{\substack{n\\ \varepsilon_n+\varepsilon_{u_2}=\varepsilon_{d_1}+\varepsilon_{d_2}}}e^3A^{(k_0,\lambda_0)*}_{u_1n}\frac{\partial}{\partial x}I_{nu_2d_1d_2}(|x|)|_{x=\varepsilon_{u_2}-\varepsilon_{d_2}}+\sum_{\substack{n\\ \varepsilon_n+\varepsilon_{d_2}=\varepsilon_{u_1}+\varepsilon_{u_2}}}e^3\frac{\partial}{\partial x}I_{u_1u_2nd_2}(|x|)|_{x=\varepsilon_{d_2}-\varepsilon_{u_2}}A^{(k_0,\lambda_0)*}_{nd_1}.\quad(46)$$

Here, $A^{(k_0,\lambda_0)*}_{n_1n_2}$ are the matrix elements of the photon wave function [Eq. (10)].

The matrix V is a complex symmetric matrix. To evaluate eigenvector of the matrix V corresponding to a reference state n_g we compose a set of configurations g including the reference state n_g and the corresponding mixing configurations, all written in the j-j coupling scheme. In this work the set g consists of all the possible configurations built on the set of electrons: $1s$, $2s$, $2p$, $3s$, and $3p$ electrons, e_R electron [see Eq. (7)], and the corresponding e_{n-1}, e_{n+1} electrons.

It is convenient to write the matrix V in block form

$$V=\begin{bmatrix}V_{11}&V_{12}\\V_{21}&V_{22}\end{bmatrix}=\begin{bmatrix}V^{(0)}_{11}+\Delta V_{11}&\Delta V_{12}\\\Delta V_{21}&V^{(0)}_{22}+\Delta V_{22}\end{bmatrix},\quad(47)$$

where the block V_{11} is constructed entirely on the states from the set g and the block V_{22} does not contain states from the set g. The blocks V_{12} and V_{21} are built with one configuration from the set g and one not included in the set g.

The matrix V_{11} can be diagonalized numerically (nonperturbatively),

$$V_{11}^{\mathrm{diag}} = B^t V_{11} B, \tag{48}$$

where B is an orthogonal matrix and B^t is the transposed matrix. The superscript t in Eq. (48) means transposition. Since in general V is a complex symmetric matrix, the matrix B is a complex orthogonal matrix,

$$B^t B = I. \tag{49}$$

Here I is a unit matrix ($I_{ij}=\delta_{ij}$) of the proper dimension.

It is convenient to compose a matrix

$$A = \begin{bmatrix} B & 0 \\ 0 & I \end{bmatrix}, \tag{50}$$

which is also an orthogonal matrix,

$$A^t A = I. \tag{51}$$

Acting by the matrix A on V yields

$$\tilde{V} = A^t V A = \begin{bmatrix} V_{11}^{\mathrm{diag}} & B^t \Delta V_{12} \\ \Delta V_{21} B & V_{22} \end{bmatrix}. \tag{52}$$

Since we have supposed that the required state n_g is weakly mixing with the states not included in the set g, the matrix $\tilde{V}$ can be diagonalized with the standard procedure [33],

$$\tilde{V}^{\mathrm{diag}} = \tilde{C}^t \tilde{V} \tilde{C}, \tag{53}$$

where the matrix $\tilde{C}$ can be built order by order. The zeroth and the first orders of the matrix $\tilde{C}$ look like

$$\tilde{C}_{ij} = \tilde{C}_{ij}^{(0)} + \tilde{C}_{ij}^{(1)} = I_{ij} + \begin{bmatrix} 0 & \dfrac{(B^t \Delta V_{12})_{ij}}{E_j - E_i} \\ \dfrac{(\Delta V_{21} B)_{ij}}{E_j - E_i} & \dfrac{(V_{22})_{ij}}{E_j - E_i} \end{bmatrix}. \tag{54}$$

The diagonalized matrices V and $\tilde{V}$ coincide, so we can write

$$V^{\mathrm{diag}} = \tilde{V}^{\mathrm{diag}} = (A\tilde{C})^t V (A\tilde{C}). \tag{55}$$

Accordingly, an eigenvector Φ corresponding to a basic function Ψ can be defined as

$$\Phi = A\tilde{C}\Psi. \tag{56}$$

Now we represent the state $n_g \in g$ in terms of a perturbation expansion,

$$\Phi_{n_g} = \sum_{k_g \in g} B_{k_g n_g} \Psi_{k_g}^{(0)} + \sum_{\substack{k \notin g \\ l_g \in g}} (\Delta V_{21})_{k l_g} \frac{B_{l_g n_g}}{E_{n_g} - E_k^{(0)}} \Psi_k^{(0)} + \cdots, \tag{57}$$

where E_{n_g} are the eigenvalues of the matrix V_{11} and $E_k^{(0)}$ are sums of the Dirac energies. The Dirac energies are assumed to incorporate the rest energy of an electron $m_e c^2$. The functions $\Psi^{(0)}$ are two-electron functions written in the j-j coupling scheme. The indices k_g, l_g run over configurations from the set g, while the index k runs over configurations not included in the set g, i.e., over all the other two-electron configurations including also the negative-energy part of the Dirac spectrum. The first term in the right-hand side of Eq. (57) can be referred to as the zero order of the employed perturbation theory; the second term represents the first order.

The numerical diagonalization of the matrix V_{11} means that in our calculation of the energies and the transition amplitudes, the one-photon exchange corrections for the specific set of electron states are included to all orders.

The radius R introduced in Eq. (5) is unambiguously related to the normalization factor N_R. In the practical calculations it is more convenient to fix the factor N_R. In this work we set it equal to $N_R=5000$ (in the relativistic units). The corresponding radius R is much larger than the radius of the area where the wave functions of the low-lying bound electrons are nonvanishing.

Accuracy of our calculation is better than 1%. The inaccuracy is determined by the approximate treatment of the higher order interelectron interaction corrections [the neglect of the matrix $\Delta V^{(2)}$ in Eq. (37)] and by the missing radiative corrections (the vertex corrections). The cross section is given by Eq. (36), where the amplitude U enters as its squared absolute value. Employing Eq. (57), the amplitude U can be written as $U=U^{(0)}+U^{(1)}+\cdots$. Accordingly, the squared absolute value of U can be written as $|U|^2=|U^{(0)}|^2+2\,\mathrm{Re}\{U^{(0)}U^{(1)}\}+|U^{(1)}|^2$. The last term corresponds to the second-order corrections and, in principle, can be omitted. Still we prefer to keep it. We consider the contribution of this term as an estimate of magnitude of the higher order corrections. The other estimate of the inaccuracy can be obtained from the comparison of calculations performed with the photon wave function [Eq. (10)] presented in different gauges: transverse (when $A^0=0$) and nontransverse. The deviation from gauge invariance is explained by the fact that the set of Feynman graphs that we take into account is not gauge invariant. The magnitude of the deviation is determined by the magnitude of the higher order corrections. We found that the transverse gauge gives slightly better convergence of the perturbation theory (the contribution of the term $|U^{(1)}|^2$ is smaller) than the nontransverse gauge. Thus, we employed the transverse gauge. Contribution of the omitted QED corrections can be estimated by comparison of the calculation performed within exact QED and within the relativistic many body perturbation theory, where the effect of retardation and the negative-energy part of the electron Dirac spectrum (in the Feynman graphs representing the interelectron interaction) are omitted.

V. RESULTS AND DISCUSSION

In Fig. 3 we present the total cross section (σ) for the capture of an incident electron by one-electron uranium ion in the ground state as a function of the energy of incident electron (ϵ_e). We give the results for the ϵ_e values above the two-electron excitation threshold. The energies are given in eV. The cross section is given in kilobarn.

Due to the dielectronic recombination the process of electron capture is a resonant process. The resonances are determined by the double excited two-electron configurations. The energies (E) and widths (Γ) of the lowest double excited

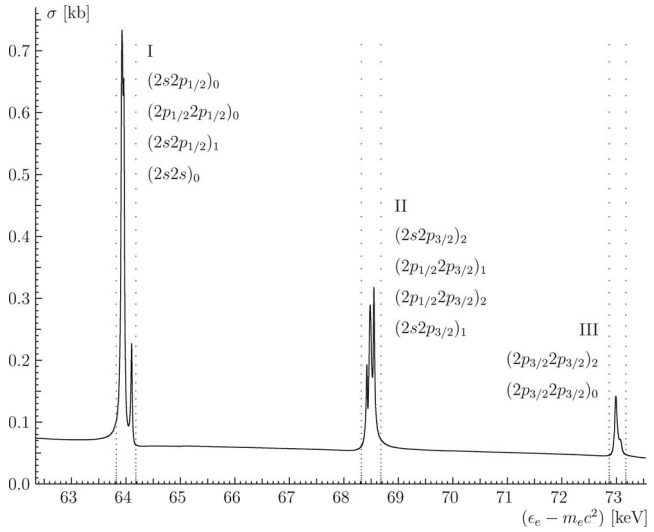

FIG. 3. The total cross section (in kb) for the capture of an incident electron by the H-like uranium ion as a function of its energy (in keV). The dotted vertical lines indicate the areas I–III enlarged in Figs. 4–6, respectively.

configurations are presented in Table III. We compare our results for energies and widths of the double excited configurations with data obtained in [9]. The accuracy of data in Table III is limited by absence of the second-order corrections of the QED perturbation theory: two-loop SE, VP corrections, and SE and VP screening corrections. These corrections have been discussed in the literature (see, for example, [16]). Note that the irreducible part of these corrections is partly taken into account [via the matrix B, see Eq. (48)]. These corrections contribute to the total energies directly, as a linear addition to the corresponding diagonal matrix element of the matrix V [Eq. (37)], and indirectly through the mixing coefficients, defined by the matrix B [Eq. (48)], for quasidegenerate configurations. For estimation of these corrections we employ results of work [34], where the "loop after loop" SESE correction is calculated for $2s$ and $2p_{1/2}$ electron states: $\Delta E_{2s}^{\mathrm{SESE}}=-0.08$ eV, $\Delta E_{2p_{1/2}}^{\mathrm{SESE}}=0.014$ eV. We estimate the two-loop SE and VP corrections by magnitude of the loop after loop SESE correction. In the case of two-electron configuration these corrections are considered for both electrons. We suppose that the missing part of the SE and VP screening corrections (for double excited configurations) is of the same order as contribution of the loop after loop SESE corrections. Accordingly, we estimate the inaccuracy of the energies in Table III as 0.25 eV for $(2p2p)$ configurations, 0.30 eV for $(2s2p)$ configurations, and 0.35 eV for $(2s2s)$ configurations. For calculation of the widths $(\Gamma=-2\,\mathrm{Im}\{E\})$ we also employed results of works [35,36], where radiative corrections to one-photon decay widths [35] $(\Gamma_{2s}^{1\mathrm{ph,rad}}=1.7\times10^{-3}$ eV, $\Gamma_{2p_{1/2}}^{1\mathrm{ph,rad}}=8.6\times10^{-2}$ eV, $\Gamma_{2p_{3/2}}^{1\mathrm{ph,rad}}=2.5\times10^{-2}$ eV) and two-photon decay widths [36] $(\Gamma_{2s}^{2\mathrm{ph}}=2.5\times10^{-3}$ eV, $\Gamma_{2p_{1/2}}^{2\mathrm{ph}}=4.1\times10^{-5}$ eV) are calculated. Accordingly, the inaccuracy of the widths is determined by the mixing coefficient (matrix B) and by the imaginary part of the SE and VP screening corrections.

TABLE III. The energies $(\Delta E=E-2m_ec^2)$ and widths (Γ) of double excited configurations of two-electron uranium in eV.

Configuration	ΔE	Γ
$(2s2p_{1/2})_0$	−67892.71(30)	31.31(4)
$(2p_{1/2}2p_{1/2})_0$	−67878.52(25)	34.35(5)
	−67878.80 [a]	33.91[a]
$(2s2p_{1/2})_1$	−67852.58(30)	31.29 (5)
$(2s2s)_0$	−67709.48(35)	28.17(5)
	−67707.91 [a]	28.49[a]
$(2s2p_{3/2})_2$	−63389.68(30)	26.18(4)
$(2p_{1/2}2p_{3/2})_1$	−63353.44(25)	57.26(6)
$(2p_{1/2}2p_{3/2})_2$	−63337.19(25)	57.27(6)
$(2s2p_{3/2})_1$	−63265.00(30)	26.20(4)
$(2p_{3/2}2p_{3/2})_2$	−58827.29(25)	52.18(6)
$(2p_{3/2}2p_{3/2})_0$	−58732.03(25)	52.04(6)

[a]Karasiov *et al.* [9].

Note that the configurations listed in Table III are excluded from the summation over the index k in Eq. (57) and, consequently, all the denominators are far from zero. If the energy of the initial state, i.e., sum of the energies of the incident electron and the one-electron uranium, becomes equal to the energy of a double excited configuration, the corresponding mixing coefficient, defined by the matrix B in Eq. (48), grows considerably. Accordingly, the maximum of the cross section is determined by the energies of the double excited configuration.

The graphs in Figs. 4–6 represent the enlarged areas in Fig. 3 with the corresponding groups of the peaks. We estimate the accuracy of our calculation as 1% (see the end of Sec. IV for the details). Contributions of the different angular momenta of the incident electron are given separately (see Table I). The recombination to the certain double excited configuration is most probable if the energy of the incident electron (ϵ_e) is equal to $E-\epsilon_{1s}$, where E is the energy of the corresponding double excited configuration and $\epsilon_{1s}=379\,184.13$ eV is the energy of the ground state of the one-electron ion of uranium. The ground state energy (ϵ_{1s}) includes the SE and VP corrections in the first order of the standard QED perturbation theory. The vertical dotted lines in Figs. 4–6 point out the energies $(E-\epsilon_{1s}-m_ec^2)$ of the double excited configurations. The maxima of the cross sections with fixed incident electron angular momenta are close to the corresponding energies of double excited two-electron configurations. The maxima of the total cross section can differ from the corresponding energies.

In Fig. 7 we compare our results with the results of the previous calculations [9,15]. A comparison demonstrates the importance of the higher-order interelectron interaction corrections even in case of H-like uranium, where these corrections should be minimal compared to the lighter ions. In the nonresonant areas the difference between our results and results in [9] is caused by the d-wave contribution to the wave function of the incident electrons taken into account in this work (see Table I). Inclusion of the Wichmann-Kroll part of the VP correction in our calculation results in the general shift of our curve to the left.

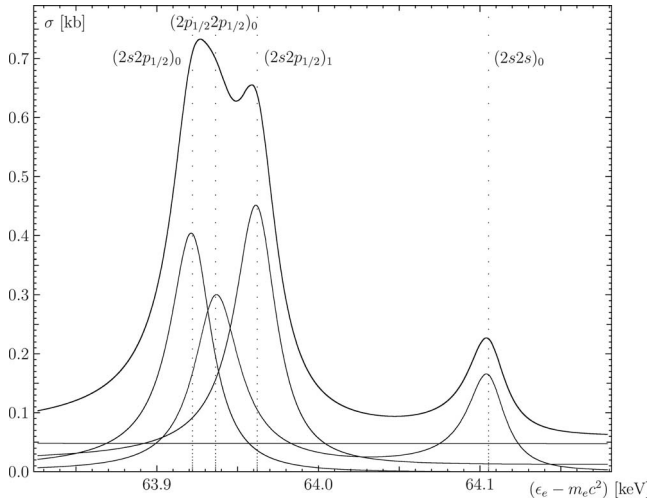

FIG. 4. The total cross section for the electron capture by the H-like uranium in energy region I (see Fig. 3). The upper curve shows the total cross section (in kb) for the capture of an incident electron as a function of its energy (in keV). The dotted vertical lines indicate the energies of $(2s2p_{1/2})_0$, $(2p_{1/2}2p_{1/2})_0$, $(2s2p_{1/2})_1$, and $(2s2s)_0$ configurations from the left to the right, respectively. The lower curves show contribution of the particular transitions (see Table I) to the total cross sections. The lower curve with maximum at $(2s2p_{1/2})_0$ energy level corresponds to transitions from $(1s,ep_{1/2})_0$ configuration. The lower curve with maxima at $(2p_{1/2}2p_{1/2})_0$ and $(2s2s)_0$ energy levels corresponds to transitions from $(1s,es_{1/2})_0$ configuration. The lower curve with maximum at $(2s2p_{1/2})_1$ energy level corresponds to transitions from $(1s,ep_{1/2})_1$ configuration. The curve with indistinct maxima represents the contribution of all the other transitions.

Though the general form of the electron spectrum remains essentially similar to the form in [9,15], the details (such as positions, height, and widths of the peaks) can differ considerably. Particularly, the difference is prominent in the areas of the resonances, i.e., where the DR process is dominant and, accordingly, the interelectron interaction plays the major role. In view of the growing accuracy of the experimental measurements this may become important especially for the ions with lower Z values.

In Fig. 8 we compare our results for rate coefficient $\alpha(\epsilon_e)$ with results reported in [5]. The rate coefficient is calculated as convolution of the cross section $\sigma(\epsilon_e)$ with a 120 eV full width at half maximum (FWHM) Gaussian [5],

$$\alpha(\epsilon_e) = v_e \frac{1}{C\sqrt{2\pi}} \int_{-\infty}^{\infty} dx \sigma(x) \exp\left[-\frac{(x-\epsilon_e)^2}{2C^2}\right], \quad (58)$$

where $v_e = \sqrt{\epsilon_e^2 - m_e c^2}/\epsilon_e$ is the incident electron velocity. The parameter C is related to the FWHM of the peak as FWHM$=2\sqrt{2\ln 2}C$. The rate coefficient is given in cm^3/s. In the experiment [5] the process of electron recombination is registered by detection of recombined ions. In the present work we suppose that the process of electron recombination is registered by detection of a photon with frequency $\omega \approx \epsilon_e + \epsilon_{1s} - E_r$, where E_r is the energy of a two-electron single excited configuration (r). In particular, we do not con-

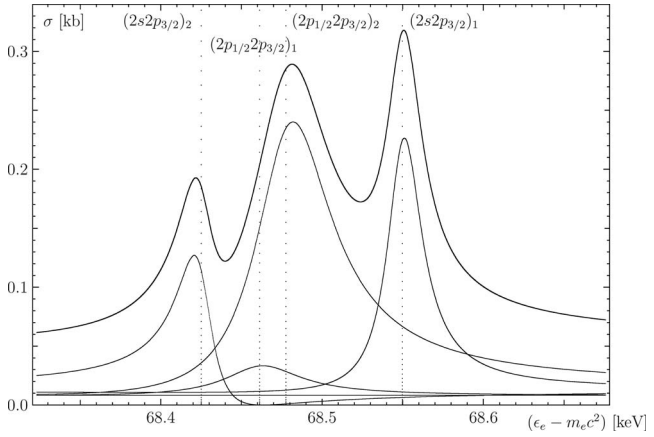

FIG. 5. The total cross section for the electron capture by the H-like uranium in the energy region II (see Fig. 3). The upper curve shows the total cross section (in kb) for the capture of an incident electron as a function of its energy (in keV). The dotted vertical lines indicate the energies of $(2s2p_{3/2})_2$, $(2p_{1/2}2p_{3/2})_1$, $(2p_{1/2}2p_{3/2})_2$, and $(2s2p_{3/2})_1$ configurations from the left to the right, respectively. The lower curves show the total cross sections for the capture of an incident electron with different angular momenta (see Table I). The lower curve with maximum at $(2s2p_{3/2})_2$ energy level corresponds to transitions from $(1s,ep_{3/2})_2$ configuration. The lower curve with maximum at $(2p_{1/2}2p_{3/2})_1$ energy level corresponds to transitions from $(1s,es_{1/2})_1$ and $(1s,ed_{3/2})_1$ configuration. The lower curve with maximum at $(2p_{1/2}2p_{3/2})_2$ energy level corresponds to transitions from $(1s,ed_{3/2})_2$ and $(1s,ed_{5/2})_2$ configurations. The lower curve with maximum at $(2s2p_{3/2})_1$ energy level corresponds to transitions from $(1s,ep_{1/2})_1$ and $(1s,ep_{3/2})_1$ configurations. The curve with indistinct maxima represents the contribution of all the other transitions.

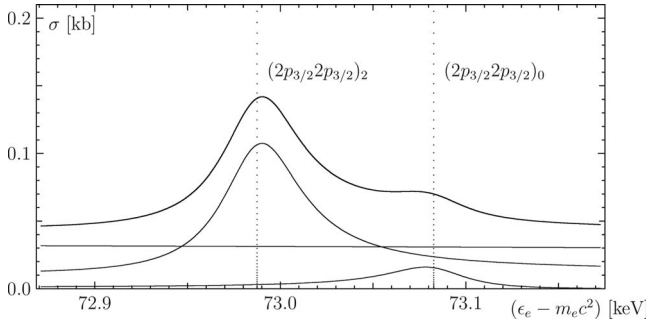

FIG. 6. The total cross section for the electron capture by the H-like uranium in the energy region III (see Fig. 3). The upper curve shows the total cross section (in kb) for the capture of an incident electron as a function of its energy (in keV). The dotted vertical lines indicate the energies of $(2p_{3/2}2p_{3/2})_2$ and $(2p_{3/2}2p_{3/2})_0$ configurations. The lower curves show the total cross sections for the capture of incident electron with different angular momenta (see Table I). The lower curve with maximum at $(2p_{3/2}2p_{3/2})_2$ energy level corresponds to transitions from $(1s,ed_{3/2})_2$ and $(1s,ed_{5/2})_2$ configurations. The lower curve with maximum at $(2p_{3/2}2p_{3/2})_0$ energy level corresponds to transitions from $(1s,es_{1/2})_0$ configuration. The curve with indistinct maxima represents the contribution of all the other transitions.

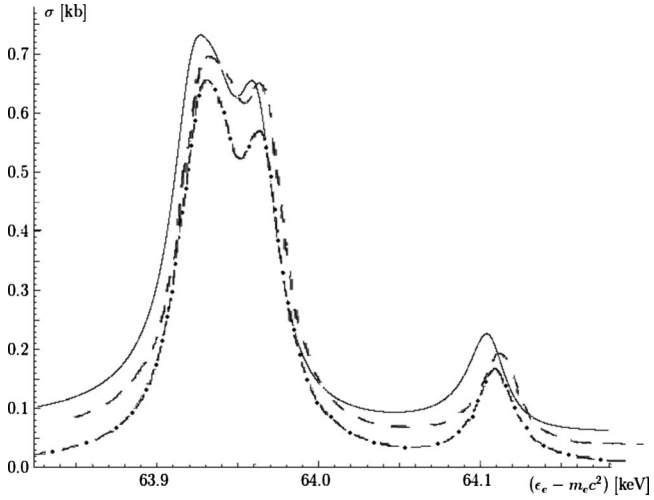

FIG. 7. The total cross section for the electron capture by the H-like uranium in the energy region I (see Fig. 3). Comparison of our calculation of the cross section with results of works [9,15]: our results are presented by the solid curve; the dashed-dotted curve represents the results of work [15]. The dashed curve shows the results of work [9].

sider a process of radiative recombination with emission of photon $\omega \approx \epsilon_e + \epsilon_{1s} - E_{(1s)^2}$, where $E_{(1s)^2}$ is the energy of two-electron ion in the ground state. Contribution of the omitted channels of recombination to the cross section and the rate coefficient within the investigated interval of incident electron energies ($\epsilon_e \in [63, 74]$ eV) is well described by a constant. Accordingly, our results must differ by the constant from results in [5] and the agreement between theory and experiment is satisfactory.

Within the framework of QED the processes of radiative recombination (RR) and dielectronic recombination (DR) are mixed. One can distinguish the RR and DR processes only in the lowest order of QED PT with respect to the interelectron interaction. Since we take into account the interelectron interaction in the higher orders of PT, we cannot show the separate contribution of the RR process.

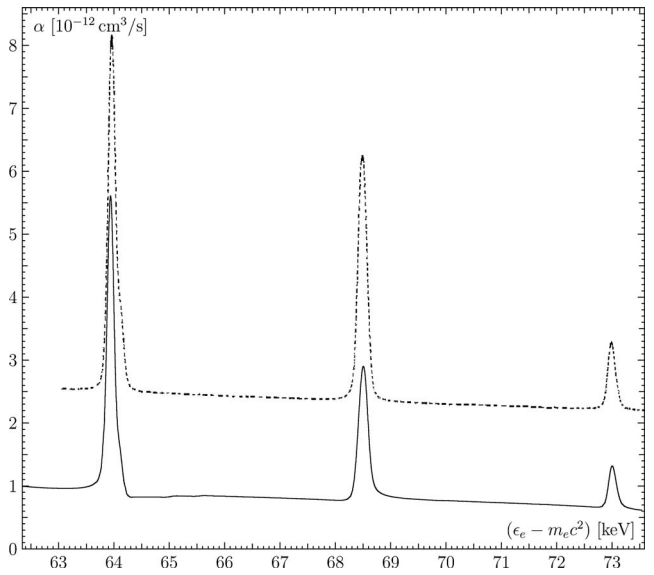

FIG. 8. Rate coefficient α (in cm^3/s) for the electron capture by the H-like uranium. Comparison of our calculation with results of work [5]: our results are presented by the solid curve; the dashed curve represents the results of work [5] (RR + DD theory curve in Fig. 2, Ref. [5]).

ACKNOWLEDGMENTS

The authors acknowledge financial support from the RFBR (Grant No. 08-02-00026-a) and from the program of development of scientific potential of high school, Ministry of Education and Science of RF (Grant No. 2.1.1./1136).

APPENDIX A: FROM CONTINUOUS SPECTRUM TO DISCRETE SPECTRUM

In this appendix we explain the physical meaning of the artificial bound electron state (e_R) introduced in Sec. II.

Eigenvectors of the Dirac equation for the point nucleus are well known [22]. The asymptotics ($r \to \infty$) of the wave function of the electron in continuum (for point or extended nucleus) reads

$$\psi_{jlm}(\boldsymbol{r}) = \frac{1}{r}\begin{pmatrix} g(r)\Omega_{jlm}(\boldsymbol{n}) \\ if(r)\Omega_{j,2j-l,m}(\boldsymbol{n}) \end{pmatrix}, \tag{A1}$$

$$g(r) = C_g \sqrt{\frac{\epsilon + m}{\pi p}} \cos[pr + \phi_g(r)], \tag{A2}$$

$$f(r) = C_f \sqrt{\frac{\epsilon - m}{\pi p}} \sin[pr + \phi_f(r)], \tag{A3}$$

where $|C_g| = |C_f| = 1$ and $\phi_g(r)$, $\phi_f(r)$ are the functions smoothly depending on r. The continuum electron function is normalized to the energy delta function.

In this appendix we compare the electron wave functions for an ion in the infinite space and the electron wave function for an ion enclosed within the box with radius R. If the ion is enclosed within a box of finite radius all the spectrum becomes discrete. For the large radius R and coordinate r the electron wave function for the ion enclosed within a box is given by its asymptotics [Eqs. (A2) and (A3)]. Accordingly, the difference between the nearest (discrete) values of the momentum (p) is defined by one half of the oscillation period of functions in Eqs. (A2) and (A3) at the border, $(r=R): \Delta pR = \pi$. Then, the difference between the nearest values of the energy (ϵ) is

$$\Delta\epsilon = \frac{p}{\epsilon}\Delta p = \frac{p\pi}{\epsilon R}. \tag{A4}$$

The equations written in this appendix should be understood in the asymptotic sense, i.e., the equations are correct up to the terms disappearing at $R \to \infty$.

Let us investigate the functions $\psi^{(\mathrm{aux})}_{e_R}(\boldsymbol{r})$ and $\psi_{e_R}(\boldsymbol{r})$ defined by Eqs. (5) and (7) and the normalization factor defined by Eq. (6) in Sec. II, respectively. For the large radius R the function $\psi^{(\mathrm{aux})}_{e_R}(\boldsymbol{r})$ can be substituted by its asymptotics [Eqs. (A2) and (A3)]. Accordingly, the squared normalization factor $(N_R)^2$ can be written as

$$(N_R)^2 = \int_0^R dr[|g(r)|^2 + |f(r)|^2] = \frac{\epsilon R}{p\pi}. \quad \text{(A5)}$$

Comparing Eqs. (A4) and (A5) we can write

$$\Delta\epsilon = \frac{1}{(N_R)^2}. \quad \text{(A6)}$$

The wave function of the electron enclosed within a box of a large radius R can be written as the function $\psi_{e_R}(\boldsymbol{r})$. The function $\psi_{e_R}(\boldsymbol{r})$ as well as the function $\psi_e(\boldsymbol{r})$ satisfies the Dirac equation. The boundary conditions at $r=R$ can be satisfied by adjusting the radius of the box R.

The integration over an interval $[\epsilon_1, \epsilon_2]$ in the continuous spectrum is equivalent to the summation over all the states (n) with the energy (ϵ_n) from the interval $[\epsilon_1, \epsilon_2]$ in the discrete spectrum (if the ion is enclosed within a sphere of radius R),

$$\int_{\epsilon_1}^{\epsilon_2} d\epsilon' F(\epsilon') = \sum_{\epsilon_n \in [\epsilon_1, \epsilon_2]} F(n), \quad \text{(A7)}$$

where function F represents some physical property (e.g., cross section). If the radius R goes to infinity, the number of discrete states in the energy interval $[\epsilon_1, \epsilon_2]$ goes to infinity and the width of the energy interval containing only one state goes to zero. Accordingly, we can write

$$F(\epsilon) = \frac{1}{\Delta\epsilon}\int_{\Delta\epsilon} d\epsilon' F(\epsilon') = \frac{1}{\Delta\epsilon}F(n) = (N_R)^2 F(n), \quad \text{(A8)}$$

where $\epsilon_n = \epsilon$ is the only discrete state inside the energy interval $\Delta\epsilon$. Thus, the transformation from the continuous to discrete spectrum results in the substitution of the continuous spectrum wave function ψ_e by the function ψ_{e_R} and in an additional factor $1/\Delta\epsilon = (N_R)^2$ to the function F (cross section), where $\Delta\epsilon$ is the distance between the nearest energy levels. Accordingly, the artificial bound electron state e_R introduced in Sec. II corresponds to the physical bound electron state (with the same energy as the electron in continuum state) of the ion enclosed within a box of a large radius R.

APPENDIX B: ELECTRON SELF-ENERGY MATRIX ELEMENTS

In this appendix we briefly represent a scheme for the first-order self-energy calculation used to evaluate both real and imaginary parts of diagonal and nondiagonal self-energy matrix elements. This procedure is well known and discussed in detail in [26,27,37] for diagonal matrix elements of the SE operator. Here, we apply it to the nondiagonal matrix elements. The Feynman graph corresponding to the first-order nondiagonal SE correction is depicted in Fig. 9(a). According to the standard Feynman rules one can write [22,38]

$$[\hat{\Sigma}(\epsilon)]_{ab} = \int d^3\boldsymbol{r}_1 d^3\boldsymbol{r}_2 \bar{\psi}_a(\boldsymbol{r}_1)\hat{\Sigma}(\epsilon;\boldsymbol{r}_1,\boldsymbol{r}_2)\psi_b(\boldsymbol{r}_2), \quad \text{(B1)}$$

where $\hat{\Sigma}(\epsilon;\boldsymbol{r}_1,\boldsymbol{r}_2)$ is the kernel of the SE operator,

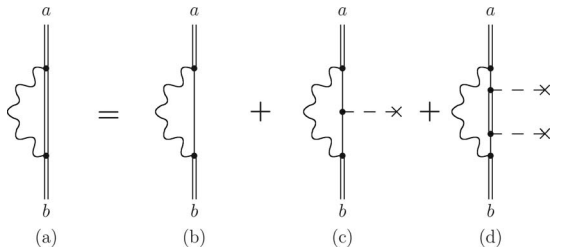

FIG. 9. Potential expansion for the electron self-energy radiative correction. The ordinary solid line corresponds to the free electron; the dashed line with the cross at the end denotes the external potential. The graphs (b)–(d) are referred to as zero-potential, one-potential, and many-potential terms.

$$\hat{\Sigma}(\epsilon;\boldsymbol{r}_1,\boldsymbol{r}_2) = e^2\frac{i}{2\pi}\int_{-\infty}^{\infty} d\omega\gamma_{\mu_1}S(\epsilon-\omega;\boldsymbol{r}_1,\boldsymbol{r}_2)\gamma_{\mu_2} \times D^{\mu_1\mu_2}(\omega;|\boldsymbol{r}_1-\boldsymbol{r}_2|), \quad \text{(B2)}$$

$D^{\mu_1\mu_2}(\omega;|\boldsymbol{r}_1-\boldsymbol{r}_2|)$ is the photon propagator in the Feynman gauge, $S(\epsilon-\omega;\boldsymbol{r}_1,\boldsymbol{r}_2)$ is the electron propagator in the Furry picture, and γ_μ are the Dirac matrices. Using the standard potential expansion of the bound electron propagator into the sum of the zero-potential [Fig. 9(b)], one-potential [Fig. 9(c)], and many-potential [Fig. 9(d)] terms, we can write

$$[\hat{\Sigma}(\epsilon))_{ab} = [\hat{\Sigma}(\epsilon)]_{ab}^{[0]} + [\hat{\Sigma}(\epsilon)]_{ab}^{[1]} + [\hat{\Sigma}(\epsilon)]_{ab}^{[2+]}. \quad \text{(B3)}$$

The first two terms in Eq. (B3) are ultraviolet divergent and require renormalization. This procedure is usually performed in momentum space according to the standard prescriptions [22]. Then,

$$[\hat{\Sigma}(\epsilon)]_{ab}^{[0]} = \frac{1}{(2\pi)^3}\int d^3\boldsymbol{p}\,\bar{\psi}_a(\boldsymbol{p})\Sigma^{\mathrm{ren}(0)}(\epsilon,\boldsymbol{p})\psi_b(\boldsymbol{p}), \quad \text{(B4)}$$

$$[\hat{\Sigma}(\epsilon)]_{ab}^{[1]} = \frac{1}{(2\pi)^6}\int d^3\boldsymbol{p}_1 d^3\boldsymbol{p}_2\,\bar{\psi}_a(\boldsymbol{p}_1)\Lambda_0^{\mathrm{ren}(0)}(\epsilon,\boldsymbol{p}_1;\epsilon,\boldsymbol{p}_2) \times V^{\mathrm{nuc}}(|\boldsymbol{p}_1-\boldsymbol{p}_2|)\psi_b(\boldsymbol{p}_2), \quad \text{(B5)}$$

where $\Sigma^{\mathrm{ren}(0)}(\epsilon,\boldsymbol{p})$ is the renormalized zero-order SE operator, $\Lambda_\mu^{\mathrm{ren}(0)}(\epsilon,\boldsymbol{p}_1;\epsilon,\boldsymbol{p}_2)$ is the renormalized zero-order vertex operator [26,37], and $V^{\mathrm{nuc}}(|\boldsymbol{p}_1-\boldsymbol{p}_2|)$ is the potential of the nucleus. After that, the integrations in zero-potential and one-potential terms can be performed numerically. A convenient version for this integration was proposed in [39]. The renormalized zero-order SE operator in the Feynman gauge is

$$\Sigma^{\mathrm{ren}(0)}(\epsilon,\boldsymbol{p}) = \frac{e^2}{4\pi}[a(\rho) + p^\mu\gamma_\mu b(\rho)], \quad \text{(B6)}$$

$$a(\rho) = 2m\left(1 + \frac{2\rho}{1-\rho}\ln\rho\right), \quad \text{(B7)}$$

$$b(\rho) = -\frac{2-\rho}{1-\rho}\left(1+\frac{\rho}{1-\rho}\ln\rho\right), \tag{B8}$$

where $p^\mu=(\epsilon,\boldsymbol{p})$ and $\rho=(m^2-p^\mu p_\mu)/m^2$. Inserting Eq. (B6) into Eq. (B4) and performing integration over angular variables one can obtain the final expression for the zero-potential term suitable for further numerical evaluation,

$$\begin{aligned}[\hat{\Sigma}(\epsilon)]^{[0]}_{ab} = \frac{e^2}{4\pi}\int_0^\infty \frac{p^2dp}{(2\pi)^3}(a(\rho)[u_a(p)u_b(p)-v_a(p)v_b(p)] \\ + b(\rho)\{\epsilon[u_a(p)u_b(p)-v_a(p)v_b(p)] \\ + p[u_a(p)v_b(p)+v_a(p)u_b(p)]\}),\end{aligned} \tag{B9}$$

where $p=|\boldsymbol{p}|$ and $u_a(p)$, $v_a(p)$ are the upper and lower radial components of the Fourier transformed wave function $\psi_a(\boldsymbol{p})$, respectively. To perform the angular integration in the one-potential term it is necessary to use the decomposition of the zero-order vertex function in the form

$$\begin{aligned}\bar{\psi}_a(\boldsymbol{p}_1)\Lambda_0^{\mathrm{ren}(0)}(\epsilon,\boldsymbol{p}_1;\epsilon,\boldsymbol{p}_2)\psi_b(\boldsymbol{p}_2) \\ = \frac{e^2}{4\pi}\{F_1^{ab}(p_1,p_2,\xi)\Omega^\dagger_{j_a l_a m_a}(\boldsymbol{p}_1)\Omega_{j_b l_b m_b}(\boldsymbol{p}_2) \\ + F_2^{ab}(p_1,p_2,\xi)\Omega^\dagger_{j_a \bar{l}_a m_a}(\boldsymbol{p}_1)\Omega_{j_b \bar{l}_b m_b}(\boldsymbol{p}_2)\}.\end{aligned} \tag{B10}$$

Here, $\xi=(\boldsymbol{p}_1\boldsymbol{p}_2)/p_1p_2$, $\bar{l}=2j-l$, and F_1^{ab}, F_2^{ab} represent the radial integrals, defined in [39] for diagonal matrix elements and generalized to the nondiagonal case. Inserting Eq. (B10) into Eq. (B5) and performing integration over angular variables one can obtain the final expression for the one-potential term suitable for the numerical evaluation,

$$\begin{aligned}[\hat{\Sigma}(\epsilon)]^{[1]}_{ab} = \frac{e^2}{(2\pi)^6}\int_0^\infty dp_1dp_2\int_{-1}^1 d\xi p_1^2p_2^2V^{\mathrm{nuc}}(q) \\ \times[F_1^{ab}(p_1,p_2,\xi)P_{l_a}(\xi)+F_2^{ab}(p_1,p_2,\xi)P_{\bar{l}_a}(\xi)]\delta_{l_a l_b},\end{aligned} \tag{B11}$$

where $q^2=p_1^2+p_2^2-2p_1p_2\xi$, $V^{\mathrm{nuc}}(q)$ is a Fourier transformation of the nuclear potential, and $P_l(\xi)$ is the Legendre polynomial.

The third term in Eq. (B3) is ultraviolet finite and can be calculated directly in coordinate space using the B-spline basis set [24,25]. The contribution of the Feynman graph depicted in Fig. 9(d) reads

$$\begin{aligned}[\hat{\Sigma}(\epsilon)]^{[2+]}_{ab} = e^2\frac{i}{2\pi}\int_{-\infty}^\infty d\omega\int d^3\boldsymbol{r}_1\ldots d^3\boldsymbol{r}_4\bar{\psi}_a(\boldsymbol{r}_1)\gamma_{\mu_1} \\ \times S^{(0)}(\epsilon-\omega;\boldsymbol{r}_1,\boldsymbol{r}_2)\gamma_0V^{\mathrm{nuc}}(\boldsymbol{r}_2) \\ \times S(\epsilon-\omega;\boldsymbol{r}_2,\boldsymbol{r}_3)D^{\mu_1\mu_2}(\omega;|\boldsymbol{r}_1-\boldsymbol{r}_4|)\gamma_0V^{\mathrm{nuc}}(\boldsymbol{r}_3) \\ \times S^{(0)}(\epsilon-\omega;\boldsymbol{r}_3,\boldsymbol{r}_4)\gamma_{\mu_2}\psi_b(\boldsymbol{r}_4),\end{aligned} \tag{B12}$$

where $S^{(0)}(\epsilon-\omega;\boldsymbol{r}_1,\boldsymbol{r}_2)$ is the free electron propagator. Angular integrations in Eq. (B12) can be performed analytically according to [40]. This yields

$$[\hat{\Sigma}(\epsilon)]^{[2+]}_{ab} = e^2\frac{i}{2\pi}\int_{-\infty}^\infty d\omega\sum_{\kappa_i L}\{j_i,j_a,L\}\frac{(-1)^{j_a-j_i+L}}{(2j_a+1)}\times\sum_{n_\alpha n_\beta n_i}\frac{R_L(\omega;a\beta\alpha b)V_{\alpha i}V_{i\beta}}{[\epsilon-\omega-\epsilon_\beta(1-i0)][\epsilon-\omega-\epsilon_i(1-i0)][\epsilon-\omega-\epsilon_\alpha(1-i0)]}. \tag{B13}$$

Here, Greek letters α, β denote the free electrons states, Latin letters a, b, i denote the electron states in the field of the nucleus, n_α, n_β, n_i are the principal quantum numbers, $\kappa_i=\kappa_\alpha=\kappa_\beta$, where $\kappa=(-1)^{l+1}(j+1/2)$ is the Dirac angular quantum number, and $\{j_i,j_a,L\}$ denotes a triangle condition for the angular momenta. $R_L(\omega;a\beta\alpha b)$ is the generalized Slater integral [40],

$$\begin{aligned}R_L(\omega;abcd) = (-1)^LC_L(\kappa_a,\kappa_c)C_L(\kappa_b,\kappa_d)\left[\int_0^\infty dx\int_0^\infty dy g_L(\omega;x,y)W_{ac}(x)W_{bd}(y)+\frac{L+1}{2L+3}\int_0^\infty dx\int_0^\infty dy g_{L+1}(\omega;x,y)Q_{ac}(x)Q_{bd}(y)\right. \\ \left.+\frac{L}{2L-1}\int_0^\infty dx\int_0^\infty dy g_{L-1}(\omega;x,y)P_{ac}(x)P_{bd}(y)\right]+(-1)^{L+1}C_L(-\kappa_a,\kappa_c)C_L(-\kappa_b,\kappa_d) \\ \times\frac{(\kappa_a+\kappa_c)(\kappa_b+\kappa_d)}{L(L+1)}\int_0^\infty dx\int_0^\infty dy g_L(\omega;x,y)V_{ac}(x)V_{bd}(y),\end{aligned} \tag{B14}$$

where

$$P_{ac}(x) = U_{ac}(x)-\frac{\kappa_a-\kappa_c}{L}V_{ac}(x), \tag{B15}$$

$$Q_{ac}(x) = -U_{ac}(x)-\frac{\kappa_a-\kappa_c}{L+1}V_{ac}(x), \tag{B16}$$

$$U_{ac}(x) = g_a(x)f_c(x)-f_a(x)g_c(x), \tag{B17}$$

TABLE IV. The matrix elements of the SE operator calculated in this work and in [29] in eV.

	This work	[29]
$1s_{1/2}$	354.99(5)	355.05
$2s_{1/2}$	65.40(2)	65.42

$$V_{ac}(x) = g_a(x)f_c(x) + f_a(x)g_c(x), \tag{B18}$$

$$W_{ac}(x) = g_a(x)g_c(x) + f_a(x)f_c(x), \tag{B19}$$

$$C_L(\kappa_a,\kappa_b) = (-1)^{j_a+1/2}\sqrt{(2j_a+1)(2j_b+1)} \times \begin{pmatrix} j_b & L & j_a \\ \frac{1}{2} & 0 & -\frac{1}{2} \end{pmatrix} \Pi(l_a,l_b,L), \tag{B20}$$

and $\Pi(l_a,l_b,L)$ is equal to unity if the sum l_a+l_b+L is even and to zero otherwise. The matrix elements of the nuclear potential are given by

$$V_{ab} = \int_0^\infty dx V^{\rm nuc}(x)[g_a(x)g_b(x) + f_a(x)f_b(x)]. \tag{B21}$$

To perform the ω integration in Eq. (B13) numerically, we rotate the contour anticlockwise around $\omega=0$ to the imaginary axis, obtaining a principal-value (PV) integral, a half-pole term (when ϵ is equal to a bound Dirac electron energy) and pole terms from the states with energies lower than ϵ, respectively,

$$[\hat{\Sigma}(\epsilon)]_{ab}^{[2+]} = [\hat{\Sigma}(\epsilon)]_{ab}^{[2+],\rm PV} + \frac{1}{2}[\hat{\Sigma}(\epsilon)]_{ab}^{[2+],{\rm pole}(\epsilon)} + \sum_{i(\varepsilon_i<\epsilon)} [\hat{\Sigma}(\epsilon)]_{ab}^{[2+],{\rm pole}(i)}. \tag{B22}$$

The expressions for the pole terms and PV integral in Eq. (B22) can be found in [40] for the diagonal matrix elements and a slight generalization to the nondiagonal case is necessary. Thus,

$$[\hat{\Sigma}(\epsilon)]_{ab}^{[2+],\rm PV} = -\frac{e^2}{\pi}{\rm Re}\left[\int_{-\infty}^{\infty} d\omega \sum_{\kappa_i L}\{j_i,j_a,L\}\frac{(-1)^{j_a-j_i+L}}{(2j_a+1)} \times \sum_{n_\alpha n_\beta n_i} \frac{R_L(i\omega;a\beta\alpha b)V_{\alpha i}V_{i\beta}}{(\epsilon-i\omega-\epsilon_\beta)(\epsilon-i\omega-\epsilon_i)(\epsilon-i\omega-\epsilon_\alpha)}\right]. \tag{B23}$$

A convenient way to organize the calculation of Eq. (B23) is to introduce a frequency-dependent effective basis set,

$$\phi_i(i\omega;\mathbf{x}) = \sum_\alpha \frac{\psi_\alpha(\mathbf{x})V_{\alpha i}}{(\epsilon-i\omega-\epsilon_\alpha)}. \tag{B24}$$

The principal-value term can be evaluated then as

$$[\hat{\Sigma}(\epsilon)]_{ab}^{[2+],\rm PV} = -\frac{e^2}{\pi}{\rm Re}\left[\int_0^\infty d\omega \sum_{\kappa_i L}\{j_i,j_a,L\} \times \frac{(-1)^{j_a-j_i+L}}{(2j_a+1)}\sum_{n_i}\frac{R_L(i\omega;a\phi_i\phi_i b)}{(\epsilon-i\omega-\epsilon_i)}\right]. \tag{B25}$$

The pole terms are

$$[\hat{\Sigma}(\epsilon)]_{ab}^{[2+],{\rm pole}(i)} = e^2\sum_L\{j_i,j_a,L\}\frac{(-1)^{j_a-j_i+L}}{(2j_a+1)}R_L(\omega;aiib), \quad \text{with} \quad \omega=\epsilon-\epsilon_i, \tag{B26}$$

and the half pole term is one half of Eq. (B26) in case $\epsilon=\epsilon_i$. The final result for the real part of the nondiagonal SE correction can be expressed in form

$${\rm Re}\{[\hat{\Sigma}(\epsilon)]_{ab}\} = [\hat{\Sigma}(\epsilon)]_{ab}^{[0]} + [\hat{\Sigma}(\epsilon)]_{ab}^{[1]} + [\hat{\Sigma}(\epsilon)]_{ab}^{[2+],\rm PV} + \frac{1}{2}[\hat{\Sigma}(\epsilon)]_{ab}^{[2+],{\rm pole}(\epsilon)} + \sum_{i(\varepsilon_i<\epsilon)}{\rm Re}\{[\hat{\Sigma}(\epsilon)]_{ab}^{[2+],{\rm pole}(i)}\}, \tag{B27}$$

and the corresponding imaginary part is

$${\rm Im}\{[\hat{\Sigma}(\epsilon)]_{ab}\} = \sum_{i(\varepsilon_i<\epsilon)}{\rm Im}\{[\hat{\Sigma}(\epsilon)]_{ab}^{[2+],{\rm pole}(i)}\}. \tag{B28}$$

In this work we calculated the nondiagonal SE matrix elements: $\langle 1s_{1/2}|\hat{\Sigma}(1s_{1/2})|2s_{1/2}\rangle$, $\langle 2s_{1/2}|\hat{\Sigma}(2s_{1/2})|1s_{1/2}\rangle$ (see Table II). Note that the nondiagonal SE matrix element yields zero if the left and right states differ by either total angular momentum or parity. In Table IV we compare our results for the real part of the SE matrix elements for $1s$ and $2s$ electrons. We also calculated the imaginary part of the SE matrix elements listed in Table II.

[1] H. S. Massey and D. R. Bates, Rep. Prog. Phys. **9**, 62 (1942).
[2] S. Mannervik, D. DeWitt, L. Engström, J. Lidberg, E. Lindroth, R. Schuch, and W. Zong, Phys. Rev. Lett. **81**, 313 (1998).
[3] C. Brandau *et al.*, Hyperfine Interact. **114**, 263 (1998).
[4] C. Brandau *et al.*, Hyperfine Interact. **114**, 45 (1998).
[5] C. Brandau *et al.*, Radiat. Phys. Chem. **75**, 1763 (2006).
[6] M. H. Chen, Phys. Rev. A **41**, 4102 (1990).

[7] M. S. Pindzola and N. R. Badnell, Phys. Rev. A **42**, 6526 (1990).
[8] P. Zimmerer, N. Grün, and W. Scheid, Phys. Lett. A **148**, 457 (1990).
[9] V. V. Karasiov, L. N. Labzowsky, A. V. Nefiodov, and V. M. Shabaev, Phys. Lett. A **161**, 453 (1992).
[10] L. N. Labzowsky and A. V. Nefiodov, Phys. Rev. A **49**, 236 (1994).
[11] A. V. Nefiodov, V. V. Karasiev, and V. A. Yerokhin, Phys. Rev. A **50**, 4975 (1994).
[12] V. M. Shabaev, Phys. Rev. A **50**, 4521 (1994).
[13] A. V. Nefiodov, L. N. Labzowsky, and D. L. Moores, Phys. Rev. A **60**, 2069 (1999).
[14] D. M. Mitnik, M. S. Pindzola, and N. R. Badnell, Phys. Rev. A **61**, 022705 (2000).
[15] S. Zakowicz, W. Scheid, and N. Grün, J. Phys. B **37**, 131 (2004).
[16] O. Y. Andreev, L. N. Labzowsky, G. Plunien, and D. A. Solovyev, Phys. Rep. **455**, 135 (2008).
[17] V. M. Shabaev, Phys. Rep. **356**, 119 (2002).
[18] W. Spies *et al.*, Phys. Rev. Lett. **69**, 2768 (1992).
[19] O. Y. Andreev, L. N. Labzowsky, G. Plunien, and G. Soff, Phys. Rev. A **64**, 042513 (2001).
[20] O. Y. Andreev, L. N. Labzowsky, G. Plunien, and G. Soff, Phys. Rev. A **69**, 062505 (2004).
[21] O. Yu. Andreev, L. N. Labzowsky, and G. Plunien, Phys. Rev. A **79**, 032515 (2009).
[22] A. I. Akhiezer and V. B. Berestetskii, *Quantum Electrodynamics* (Wiley Interscience, New York, 1965).
[23] D. A. Varshalovich, A. N. Moskalev, and V. K. Khersonskii, *Quantum Theory of Angular Momentum* (World Scientific, Singapore, 1988).
[24] W. R. Johnson, S. A. Blundell, and J. Sapirstein, Phys. Rev. A **37**, 307 (1988).
[25] V. M. Shabaev, I. I. Tupitsyn, V. A. Yerokhin, G. Plunien, and G. Soff, Phys. Rev. Lett. **93**, 130405 (2004).
[26] N. J. Snyderman, Ann. Phys. **211**, 43 (1991).
[27] S. A. Blundell and N. J. Snyderman, Phys. Rev. A **44**, R1427 (1991).
[28] I. Goidenko and L. Labzowsky, in *Fundamental World of Quantum Chemistry*, edited by E. J. Brändas and E. S. Kryachko (Kluwer, The Netherlands, 2004), Vol. III, p. 407.
[29] T. Beier, P. J. Mohr, H. Persson, and G. Soff, Phys. Rev. A **58**, 954 (1998).
[30] A. N. Artemyev, V. M. Shabaev, V. A. Yerokhin, G. Plunien, and G. Soff, Phys. Rev. A **71**, 062104 (2005).
[31] P. J. Mohr, G. Plunien, and G. Soff, Phys. Rep. **293**, 227 (1998).
[32] T. Beier, G. Plunien, M. Greiner, and G. Soff, J. Phys. B **30**, 2761 (1997).
[33] L. D. Landau and E. M. Lifshits, *Quantum Mechanics* (Pergamon, Oxford, 1977).
[34] A. Mitrushenkov, L. Labzowsky, I. Lindgren, H. Persson, and S. Salomonson, Phys. Lett. A **200**, 51 (1995).
[35] J. Sapirstein, K. Pachucki, and K. T. Cheng, Phys. Rev. A **69**, 022113 (2004).
[36] L. N. Labzowsky, A. V. Shonin, and D. A. Solovyev, J. Phys. B **38**, 265 (2005).
[37] V. A. Yerokhin and V. M. Shabaev, Phys. Rev. A **60**, 800 (1999).
[38] L. Labzowsky, G. Klimchitskaya, and Yu. Dmitriev, *Relativistic Effects in the Spectra of Atomic Systems* (Institute of Physics, Bristol, Philadelphia, 1993).
[39] V. A. Yerokhin, A. N. Artemyev, T. Beier, G. Plunien, V. M. Shabaev, and G. Soff, Phys. Rev. A **60**, 3522 (1999).
[40] S. A. Blundell, Phys. Rev. A **46**, 3762 (1992).